Comparative Model Evaluation with a Symmetric Three-Link Swimming Robot

Brian J. Van Stratum, Max P. Austin, Kourosh Shoele, and Jonathan E. Clark

***Abstract*— In this paper we present swimming and modeling for Trident, a three-link lamprey inspired robot that is able to climb on flat smooth walls. We explore two gaits proposed to work for linear swimming, and three gaits for turning maneuvers. We compare the experimental results obtained from these swimming experiments with two different reduced order fluid interaction models, one a previously published potential flow model, and the other a slender cylinder model we developed. We find that depending on the the parameters of swimming chosen, we are able to move forward, backward and sideways with a peak speed of 2.5 cm/s. We identify the conditions when these models apply and aspects that will require additional complexity.**

I. Introduction

Snake and snake-like animals (eels, lampreys, etc.) are able to move through an amazing variety of natural and man-made environments utilizing a rich set of locomotion strategies or gaits. They can slither, crawl, swim, glide, and even climb vertical walls! These animals have, in turn, inspired the design and control of limbless robots that have shown impressive performance both on land and in water. Example of this include ACM-5 [1] which has demonstrated the ability to swim and slither on land, the Reel [2] robot, which used gaits revealed by geometric mechanics, and Amphibot [3] which can transition from land to water using a robust CPG based control policy. Snake robots have even demonstrated swimming in granular media, and traversing sandy slopes [4], [5]. These robots generally leverage their high degree of articulation to produce biologically mimetic behaviors.

In this paper we focus on adding swimming capabilities to robots such as the lamprey-inspired multi-modal robot shown in Fig. 1. As shown in Fig. 1 (left), the Pacific Lamprey or *Lampetra Tridentata* is an eel-like fish that can use its sucker-like mouth to adhere to and climb vertical surfaces, allowing it to scale waterfalls or weirs as they swim upstream in fresh water to spawn [6]. Inspired by this, the recently developed Trident climbing robot [7] Fig. 1 (top right), is a 3-link robot capable of dynamic climbing up slopes of up to 70°. Based on insights from a simple 3-link reduced order dynamic model, the robot has been able to show comparable climbing behaviors to the Pacific Lamprey.

When well designed, this type of low dimensional system can enable insights and show performance which may be obscured or difficult to achieve in higher dimensional systems. This has been seen in bio-mechanical models of legged running and climbing [8]–[10]. In addition, limbless high DOF systems have also been usefully described by a dimensionally collapsed set of parameters [11], [12]. These reduced order models have shown excellent performance in terrestrial robots [4], [13], [14].

FAMU/FSU College of Engineering, Tallahassee, FL 32310 email:bjv02@fsu.edu jeclark@fsu.edu

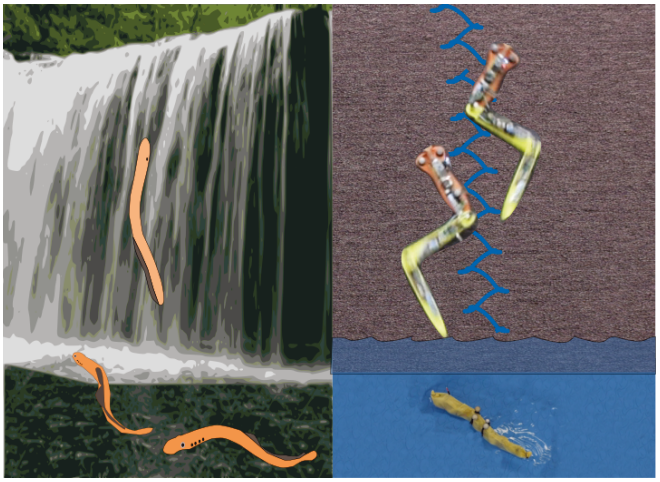

Fig. 1: Not-yet-multimodal Trident wall climbing robot is inspired by the unique swimming and climbing abilities of the Pacific Lamprey.

This leads us to ask if there are simple aquatic models that could be used to develop design and control insights for swimming, Fig. 1 (bottom right), and that could be used in conjunction with these terrestrials models for integrated, multi-modal control and planning purposes.

Due to the complexity of the fluid dynamic driven locomotion, researchers have endeavored to use several different models to predict limbless locomotion/swimming. These techniques include Purcell's swimmer (neglecting viscosity) [15], Lighthill's model, drag and added mass models based on Morison's equation, and computational fluid dynamics [2], [16]–[19], with each representing an increased level of complexity for modeling fluid structure interactions.

For low Reynolds numbers, the simplest swimmer is the two DOF Purcell's swimmer with known optimal swimming trajectory [20]. Considering a simple three link swimmer such as Purcell's swimmer is common in geometric mechanics as in several numerical studies [18], [21]–[24] and higher DOF [25], [26] serial mechanisms for both terrestrial and swimming motions. A recent simulation study demonstrated optimized control for a 5-link model subject to coulomb friction and a viscous environmental models [17]. Lighthill proposed an elegant model that captures the reactive effect of water in carangiform and anguilliform swimming.

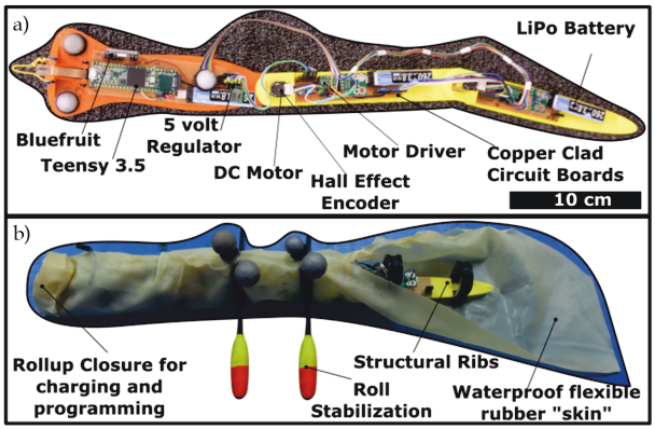

Fig. 2: (A) Trident cutaway view of essential climbing hardware. Trident is a three piece power autonomous robot driven by DC motors and equipped with electronics for data logging. (B) Trident in the process of being water proofed with a latex rubber skin for swimming. Ribs are added for structure and the addition of roll stabilizing floats

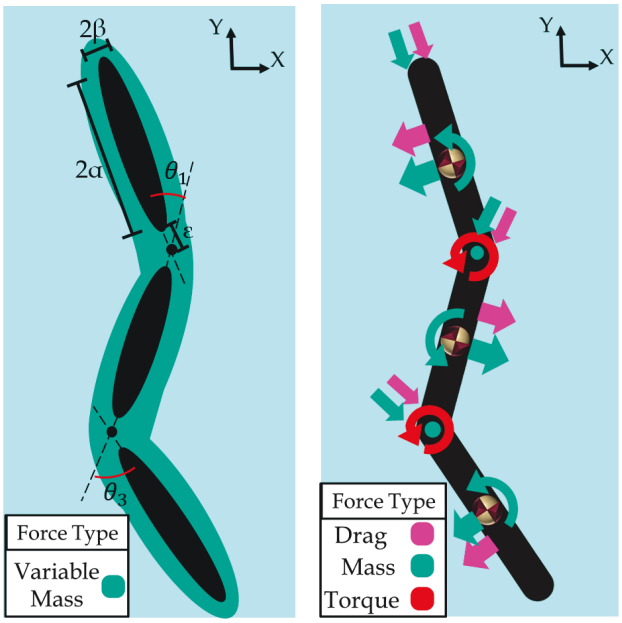

A) Potential Flow Model B) Slender Cylinder Model

Fig. 3: 3-link models used in simulation.

Morison's equations allow the fluid interaction to be replaced with added drag and added mass elements and has been applied to swimming segmented snake robots with success [27], [28]. Although several of these models have been expanded to inform the control of highly articulated limbless robots, very few have been tested on robots in their low degree of freedom state.

In this work, we evaluate the efficacy of two styles of reduced order models for swimming with 3-links: a frequently cited potential flow model (PF) and a slender cylinder (SC) model based on Morison's equations. We choose these two models to evaluate as they capture two of the primary fluid effects for locomotion: added mass and drag forces. In addition, they are simple, computationally efficient and may easily be combined with terrestrial models for multi-modal control and planning. We further identify facets of the robot's motion that these models accurately capture and elements that will require additional complexity.

The remainder of the paper begins with a description of the Trident hardware platform (Sec. II) and describes how it is adapted from its climbing form to swimming. In Sec. III the models used in simulation are described, including the derivation of the three link slender cylinder model and an explanation of the controllers. We subsequently (Sec. IV) evaluate these model predictions in hardware for both forward swimming and turning. Section V summarizes insights from our experimental model verification and outlines future areas of work.

II. Robot Design

The hardware platform used in this work, Trident (Fig. 2), was adapted in order to test and compare the three link models and demonstrate swimming gaits in hardware. Trident is a 360 gram robot composed of three 3D printed ABS segments connected and driven by two Pololu DC Micro Metal Gear Motors with a 150:1 gear head and quadrature encoders. The motors combined output shaft resolution is 1800 counts per revolution. Trident's link length ($182mm$) was chosen to optimize jumping performance as documented in [29]. Both joints are capable of a range of motion of $\pm 90^\circ$ measured from the previous link's centerline. Trident is equipped with microspines for climbing, but for swimming trident is provided a rubber skin wrapped around and secured by rubber cement with outriggers on the middle link for roll stabilization.

Trident is controlled by a Teensy 3.5 microcontroller with active communications facilitated by an Adafruit Bluefruit SPI Friend. Trident is equipped with a Pololu current sensor for computing motor torque. On-board data logging (of joint angles, currents, and voltages) and motor position control (using trajectories in Sec. III-D) occurs at 1kHz. System power is supplied by three LiPo batteries connected in series forming a nominal 11 volt bus.

III. Modeling

The potential flow model (PF) and the slender cylinder (SC) model selected to be evaluated against the behavior of the robot are outlined below.

A. Potential Flow Model

The potential flow (PF) model (Fig. 3A) used is identical to the model made by Melli et al. [18], [30]. This is a nondimensional model made up of three close ellipses which are connected via pin joints at the intersection of each serial link. The physical parameters of this model include the ellipse major (α) and minor (β) axes lengths and the length to the virtual pivot point (ϵ). The primary driving force in this model is a variable added mass which is computed

Variable	Symbol	Val.	Unit
Linkage Mass	m	120	g
Linkage Length	L	0.18	m
Submerged Width	w	0.015	m
Stall Torque	τ_S	0.25496	Nm
No-load speed	ω_{nl}	22.52	rad/s
Water Density	ρ	997	kg/m^3
Total Length Drag Coeff.	C_{dL}	135.5	kg/m
Total Front Drag Coeff.	C_{df}	27.5	kg/m
Length Added Mass	m_{LL}	4.945	kg
Front Added Mass	m_{ff}	2.27	kg
Rotational Added Mass	$m_{\theta\theta}$	0.00766	kgm^2
Controller Stiffness	k	5	Nm/rad
Controller Damping	b	0.25	Nms/rad
Maximum Angle	θ_{max}	39	deg
Offset Angle	θ_O	9	deg
Control Period	τ_p	1.38	s
Duty Factor	$Duty$	22	%

TABLE I: Default Simulation Parameters

instantaneously for each change in geometry. Geometric changes are fully-controlled, time-variant angles of the front and rear link relative the central link (θ_1, θ_3). Simulations of this model are modified from an available code base [30] to match robot parameters.

B. Slender Cylinder Model

The second model of 3-link lamprey robot is a slender cylinder (SC) model (Fig.3b) in which the effects of the interactions between the fluid and the body are decomposed to a set of simplified forces, namely drag, added mass, motor torques and resulting reaction forces. The model is made up of three rigid cylinders connected via torsionally actuated pin joints. The states of the system are the global Cartesian position and angle x, y, θ_2 of the middle link and the relative angles of front and rear link with respect to the center θ_1, θ_3. Each linkage ($n = 1, 2, 3$) is subjected to a drag force ($F_D n$) in both its radial and transverse directions.

$$F_{Dn} = -R_{nG}(C_d\, R_{nG}^T\, \dot{p}_{nG} |R_{nG}^T\, \dot{p}_{nG}|) \tag{1}$$

$$C_d = \begin{bmatrix} C_{df} \\ C_{dL} \\ 0 \end{bmatrix}$$

The drag force (Eq. 1) can be expressed as a function of the time derivative of the linkages' instantaneous position in the world frame (p_{nG}) and the combined drag coefficients (C_d) along the radial and transverse directions, which combine the unitless drag coefficients, fluid density, and areas. These forces are rotated into the global Cartesian frame from the frame of link n via the rotation matrix R_{nG}. The transverse drag forces act at the center of pressure L_{cpn} of the link, while the radial drag force is located at the centroid.

Each linkage also experiences a simplified added mass force F_{An}.

$$F_{An} = -R_{nG}(M_a\, R_{nG}^T\, \ddot{p}_{nG}) = -M_{addn}\, \ddot{q} - F_{AnV}$$

This force is a function of the second derivative of the linkages' instantaneous position in the world frame and the added mass tensor of the object M_a. For simplicity, only the main diagonal elements (m_{ff}, m_{LL}, and $m_{\theta\theta}$) of this mass tensor are considered in this model and do not vary with configuration. This force can be expressed as a resultant added mass matrix M_{addn}, which affects the second derivative of the system state vector, $q = [x, y, \theta_2, \theta_1, \theta_3]^T$, and a force proportional to coupled velocities F_{AnV}.

Reaction forces F_{Rn} and moments τ_{R2} occur at the pin joint connections with the center link.

$$F_{Rn} = -R_{nG}(M_n\, R_{nG}^T\, \ddot{p}_{nG}) = -M_{Rn}\, \ddot{q} - F_{RnV}$$

$$\tau_{R2} = 0.5 R_{2G}(\begin{bmatrix} L \\ 0 \\ 0 \end{bmatrix} \times (F_{R1} + F_{D1} - F_{R3} - F_{D3}))$$

Like added mass forces, the reaction forces can be broken down into an acceleration dependant mass matrix M_{Rn} and velocity dependant force F_{RnV}. These reactions, in addition to the drag forces on the links, act at the connections of the second link and create equivalent moments τ_{R2}.

From these the equations of motion can be derived using Newton's method.

$$\Sigma F = \begin{bmatrix} \Sigma F_{Dx} - \Sigma F_{AnVx} - \Sigma F_{RnVx} \\ \Sigma F_{Dy} - \Sigma F_{AnVy} - \Sigma F_{RnVy} \\ \Sigma F_{dL2} + \tau_{R2} + \tau_1 + \tau_3 \\ L_{cp1} F_{dL1} - \tau_1 \\ L_{cp3} F_{dL3} - \tau_3 \end{bmatrix}$$

$$(M + M_{add} + M_R)\ddot{q} = \Sigma F$$

In the above equations, the drag forces in the transverse directions on each link are noted as F_{dLn}. The applied torques at the pin joint connecting link 1 and 2 and connecting link 2 and 3 are denoted τ_1 and τ_3 respectively. The centers of pressure of the drag force for links 1 and 3 are L_{cp1}, L_{cp3} respectively.

C. Model Parameters

The parameter values for the simulated models are shown in Table I. Physical parameters of the model, such as linkage mass and length, are taken directly from robot measurements. In this design, these values are identical for each linkage. The nondimensional parameters for the PF model are taken from the physical parameters setting $\alpha = 1$ and $\epsilon = 0.1$ which together make up the total nondimensional linkage length. A linear motor model was used to limit the applied torques of the SC model by its stall torque τ_S and no-load speed ω_{nl}.

Fluid parameters of the model are computed from experimental testing. Linear drag (C_{dL} & C_{df}) and added masses (m_{LL} & m_{ff}) are derived from experiments with a variable weight pulley system towing the robot in a long tank. Center of mass velocities and acceleration tests are captured via a $300Hz$ Vicon motion capture system. The combined drag forces are computed from a force balance at the steady state velocity assuming a lossless pulley. The drag data was curve fit with an 0.970 R^2 value. The linear mass was computed from the acceleration phases of the pulley system with the chosen mass selected from the median of this range. The rotational added mass $m_{\theta\theta}$ (which included the gearbox

inertia) was computed using a motor spin-down test with a dummy Trident link attached. Added mass for the head and tail link is calculated with parallel axis theorem and link rotations about their end points.

D. Model Control

To find locomotive behaviors in the models, two controllers were employed in simulation: a sinusoidal and a Buehler-clock based rowing controller [31]. The sinusoidal control varied the commanded position of the joints (θ_{nDes}) using phase offset sinusoids (Fig. 4a-insert). That is $\theta_{nDes} = \theta_O + (\theta_{max}) * \sin(2\pi/\tau_P t + \phi)$, where ϕ is an offset between the motors. The Buehler-clock based controller linearly interpolates between an offset θ_O and maximum θ_{max} angle with a time differential ratio $Duty$ between the power stroke (θ_O to θ_{max}) and the recovery stroke (Fig. 4d-insert). For the SC model, these are applied as torques to the joint angles through a PD controller, where: $\tau_n = -k(\theta_n - \theta_{nDes}) - b(\dot{\theta}_n - \dot{\theta}_{nDes})$.

E. Model Behaviors

The two models are integrated numerically using a fourth and fifth order Runge-Kutta algorithm. The simulation results for the PF model are re-dimensioned to the robot's scale for comparison. In the PF model (as in previous works [18]) an undulating gait was seen (Fig. 4a) when using the sinusoidal control with a fixed phase shift between the front and rear wave forms. The SC model was found to produce repeatable rowing gaits when using the Buehler-clock control with the joints biased to one side (Fig. 4d).

Interestingly, neither model produced the same behaviors as the other when using the same controllers. When using the rowing control on the PF model at identical parameters, the model only slides back and forth near perpendicular to its center. Similarly when the SC model attempts the undulating gait, it instead rotates and translates sideways while turning. Both behaviors were tested on the robot hardware to evaluate each models' accuracy.

IV. Experimental Swimming Tests

To evaluate swimming performance, five behaviours were chosen to study experimentally: two forward swimming gaits (Fig. 4) and three turning gaits (Fig. 6). Early tests and subsequent hardware optimizations were each run for 20 seconds and the displacement and timing was measured by hand. All presented center of mass and orientation data was captured using a seven camera, $300Hz$ Vicon motion capture system tracking the center link with tests run for at least eight strokes in a round 1 meter diameter by 0.15 meter deep pool.

A. Forward Translation Testing

The two models' accuracy were tested by employing both controllers in hardware. Varying sets of control parameters were used in hardware to find achievable swimming motions. Examples of the simulated behaviors predicted on the robot are shown in Fig. 4. The sinusoidal controller used in the PF model (Fig. 4b-c) was about 10 times slower

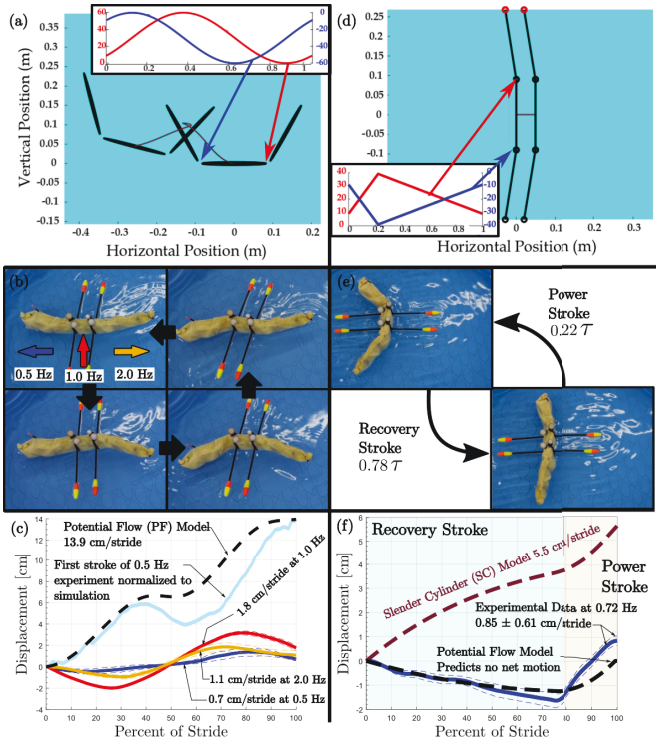

Fig. 4: Simulation and experimental results for swimming with (a-c) a sinusoidal and (d-f) a rowing control policy. (a) Simulated single stride displacement. Insert shows the control trajectories. (b) Four stages of Trident executing a gait. (c) Single stride displacement profiles at various frequencies. Colored dashed lines represent the mean $\pm\sigma$ for $N = 8$. Also shown is the first stroke normalized to PF predicted displacement. (d) Simulated displacement and target trajectory for the rowing gait discovered using the SC model. (e) Trident executing the rowing gait. (f) Single stride displacement experimental data $N = 16$ vs SC and PF model.

than predicted, with peak speeds of 1.8cm/s (vs. 14 cm/s expected). Furthermore, the directions of these motions were not consistent with the model and showed distinct, unmolded, frequency dependence, with $0.5\,Hz$ moving as predicted by the PF model, at $2\,Hz$ moving the opposite direction, and $1\,Hz$ moving sideways. These directions are color coded and shown in Fig. 4b.

The PF model does, however, capture the displacement trend during the first 3 strokes when the swimmer moves forward at $< 0.5cm/s$ (corresponding to Reynolds number $\approx 3\times10^3$). Figure 4c includes a cyan trace for the first stroke of the $0.5\,Hz$ swimming test. This is normalized to the PF model trace for better comparison. This trend change with speed explains why the error bars are wider for the $0.5\,Hz$ test in Fig. 4c when compared to the error bars of the higher frequency swimming. The PF model not including velocity-dependent drag terms may explain why the model predicted speeds for the PF model were $8-20$ times faster.

Figure 4e&f shows the experimental results of Buehler-

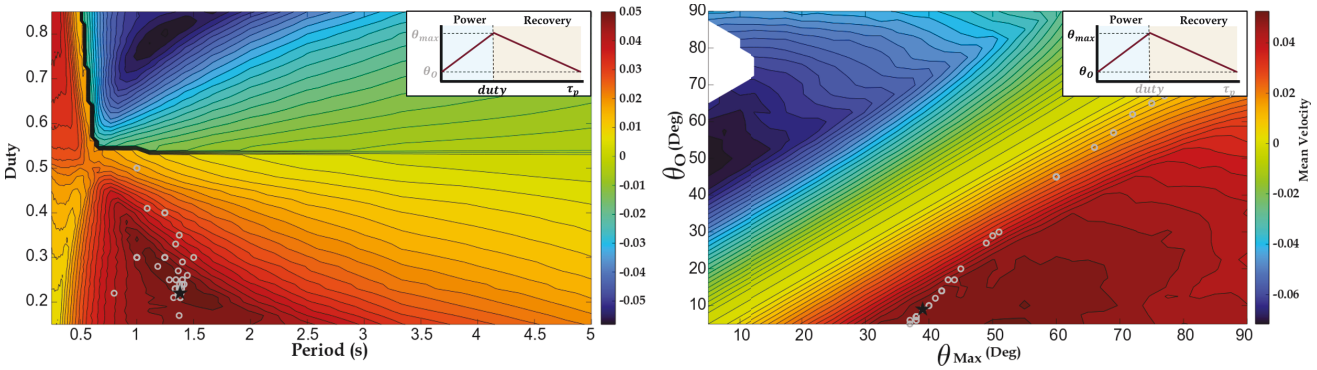

Fig. 5: 2D Model cross sections of velocity as a function of control parameter variation for the SC simulation of the rowing model. The hardware optimizes results are shown as a black star. The 36 grey dots indicate experimental data points generated as part of the Nelder-Mead direct optimization.

clock rowing controller. In Fig. 4f the displacement predicted by both models is shown. Note that the PF model trend compares favorably except for that it predicts no net motion. While the PF model using a rowing controller erroneously predicts a zero forward velocity, it does capture the robot's deceleration during the recovery stroke. The SC model also over predicts swim speed by $2.2-6.5$ times, but the direction of travel is correct and consistent. It underestimates losses during the recovery stroke, but there is much greater accuracy in the power stroke. These results suggests that a future synthesis of these models may better capture the rowing behaviors.

B. Parameter Variation and Optimization

To further evaluate the SC model's predictive ability, model based parameter variations are compared with an experimental Nelder-Mead optimization. The Nelder-Mead optimized the control parameters of the Buehler clock gait: θ_O, θ_{max}, τ_P, and $duty$. These optimization experiments were run in a rectangular $2.4\,m \times 1.2\,m$ by $0.3\,m$ deep pool and commanded to run for $20\,s$ starting from rest. The net forward displacement was measured and maximized (i.e. $min[-\Delta X]$) in optimization. The algorithm coverged after 36 iterations. The resulting optima converged to a gait with parameters $\theta_O = 9°$, $\theta_{max} = 39°$, $\tau_P = 1.38s$, and $duty = 0.22\%$ and traveled at and average of $2.5\,cm/s$ under these test conditions.

These results are compared to two control 2D parameter variations of the SC model around the optimal point. These sweeps vary timing variables (period from $0.25s - 5s$ and duty factor from $15\% - 85\%$) and the angular limits (from $0 - \pi/2$). Average velocity over 10 strokes (starting from rest) was recorded for each control case with outlier areas (caused by numerical errors during integration) removed.

The results of this sweep are shown in Fig. 5 along in-plane projections of the experimental simplex member locations. Simplex members depict a descent into the locally optimal region from the hardware optimization. The hardware optimum was in the highest speed region of the timing sweep and the second highest speed region of the actuation angle sweep. This agreement suggests that the SC model captures the qualitative effect of parameter variation for forward swimming with a rowing gait.

C. Turning and Maneuverability

To generate swimming maneuverability on Trident three turning behaviors were tested. One turn, suggested by the PF model, is induced by placing a fixed angular offset on the sinusoidal controller (Fig. 6a). This was tested at three different stroke frequencies ($0.5, 1$, and $2Hz$) and compared with the PF model (Fig. 6b). It was found PF modelled turn only rotated in the predicted direction at the highest frequency tested, and at the end of this stride frequency the turn magnitude was two orders of magnitude below the predicted value. Furthermore, the shape of the predicted motion significantly diverges from the robot after 35% of the stroke. These results suggest that, at least at the Re seen by our robot, this model does not accurately predict turning.

From extensive parameter sweeps that induce asymmetry in the Buehler-Clock controller, two turn styles were chosen for robot testing, one efficient limping turn (Fig. 6c) and a small radius Z-turn (Fig. 6e).

The limping turn gaits (Fig. 6d) induced turns in the directions the models predicted, but at only 1/5 of the magnitude. The profiles of the robot's turns shows similarity to the models predictions, just with smaller magnitudes and overshoot during the first 20% of the stride. This is likely from an overestimate of the fluid forces, with the overshoot emerging from a greater inertial effect than seen by the robot.

The Z-turn (Fig. 6f) showed the fastest and sharpest turns achieved by the robot (turning up to $10°$ per stroke) however the rotation direction is inverted from both the PF and SC model predictions. Experiments with model parameters (such as increasing C_{dL}) found that the same direction turns to the robot were achievable but not only at moderate angles. These results suggest that the driving fluid dynamic effect for this turn is not captured in either of these models alone.

Though for the froward rowing behaviors these models may be improved through fusion of their propulsive effects, it appears that for turning there may be another effect that needs incorporation.

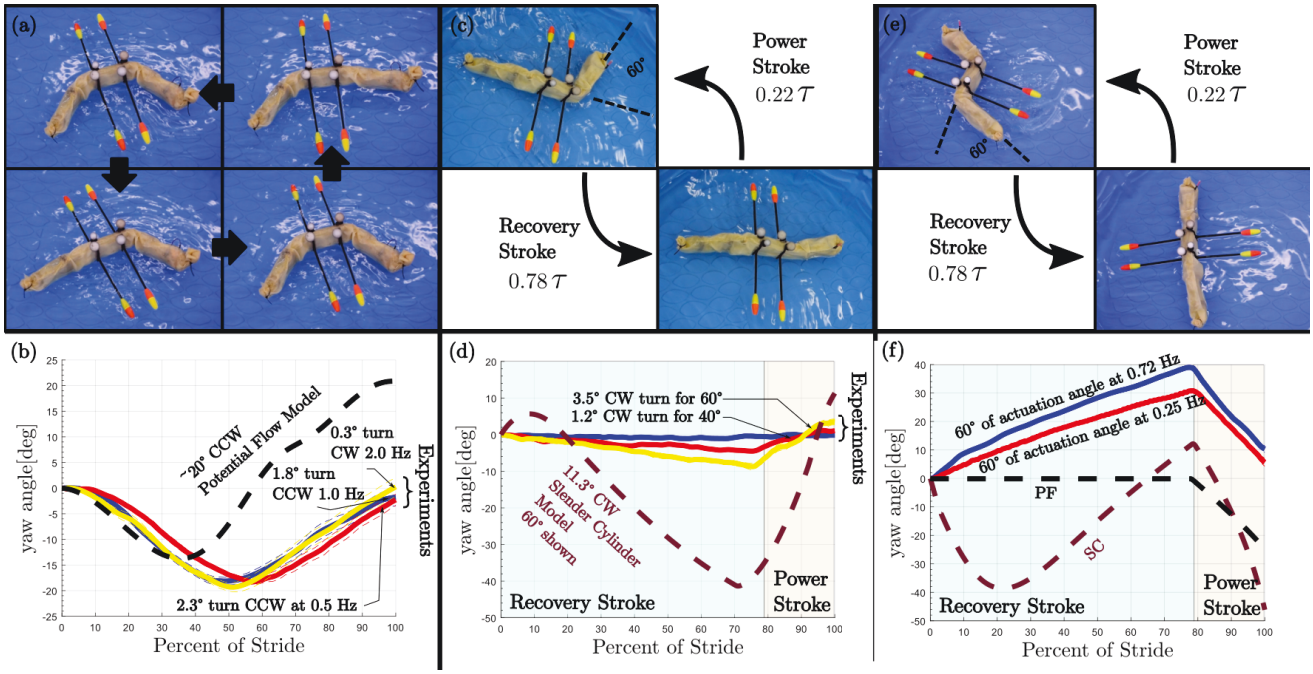

Fig. 6: (a) Trident executing the turning gait proposed by melli. (b) Experimental Yaw angle results compared against the PF model simulated turning. (c) Trident executing the turning behaviour revealed by the SC model. (d) Experimental Yaw angle data showing a peak change in yaw angle for 60° link strokes. (e) Trident executing a Z-turn discovered experimentally. (f) Experimental, PF and SC yaw angle data for the Z-turn. All tests consisted of $N = 9$ strokes.

V. Conclusions and Future Work

This paper presents a comparative hardware analysis of two 3-link swimming models (a potential flow model and a slender cylinder model) for the purposes of enabling swimming on the Trident climbing robot. The mechanics of each of these models' propulsion are described. The models are shown to predict differing motions under identical control parameters, with forward motion in the PF model to consist of forming loops in the shape space while the SC model does so by creating a bias velocity differential. When tested on the hardware, the SC model was found to produce reliable rowing behaviors in directions predicted by the model (though at lower speeds). The PF model was also optimistic as to the magnitude of displacement and rotation, additionally some direction result were contrary to the model. Our results would support the assertion that the PF model assumptions with respect to drag are more valid at Reynold's numbers less than 3×10^3, but more data is needed for clarity here. Further, parameter variations of the SC model predict optimal performance in the rowing motions of the robot. Three model predicted turns styles (a bias sine wave, limping, and Z-turn) were also tested. It was found that the SC model correctly predicted the directions of the limping turns but overpredicts turn rates. Center of mass profiles from both the rowing behaviors and limping turns suggest that, although good at predicting direction and speed trends, the SC model may benefit from the shape variable added mass effect of the PF model particularly with managing inertial effects during the recovery stroke. It was found that for the Z-turn, although fast in hardware, is predicted by neither model correctly, suggesting that more complex fluid models will be required to capture its motions.

In the future, we would also like to look towards exploring other reduced order fluid models for comparison. The reverse swimming direction discovered at two Hz for PF control policy Fig.4c as well as other behaviours would likely be predicted by Lighthill's model. We intend to synthesize the insights of these various models and hardware results to inform the design of a new model which is able to capture several behaviors of a segmented body swimmer while maintaining the computational speed and low-parameter benefits of reduced order models. Using this model, we hope to be able to design optimal control policies for segmented link swimming. We would also like to expand the robots capabilities to enable transitions from swimming to vertical climbing, possibly through the used of soft actuators to minimize electromechanical failures.

Acknowledgment

We would like to thank Justin Cheeseborough and Roshard Jackson for their assistance with collecting experimental data. This work was funded by the National Science Foundation Expanding Frontiers in Research and Innovation Program, grant number 1935278.

REFERENCES

[1] B. Li, S. Ma, C. Ye, S. Yu, G. Zhang, and H. Gong, "Development of an amphibious snake-like robot," in *2010 8th World Congress on Intelligent Control and Automation*. IEEE, 2010, pp. 613–618.

[2] K. A. McIsaac and J. P. Ostrowski, "Motion planning for anguilliform locomotion," *IEEE Transactions on Robotics and Automation*, vol. 19, no. 4, pp. 637–652, 2003.

[3] A. Crespi and A. J. Ijspeert, "Amphibot ii: An amphibious snake robot that crawls and swims using a central pattern generator," in *Proceedings of the 9th international conference on climbing and walking robots (CLAWAR 2006)*, no. CONF, 2006, pp. 19–27.

[4] H. Marvi, C. Gong, N. Gravish, H. Astley, M. Travers, R. L. Hatton, J. R. Mendelson, H. Choset, D. L. Hu, and D. I. Goldman, "Sidewinding with minimal slip: Snake and robot ascent of sandy slopes," *Science*, vol. 346, no. 6206, pp. 224–229, 2014.

[5] J. Dai, H. Faraji, C. Gong, R. L. Hatton, D. I. Goldman, and H. Choset, "Geometric swimming on a granular surface." in *Robotics: Science and Systems*, 2016, pp. 1–7.

[6] P. Kemp, T. Tsuzaki, and M. Moser, "Linking behaviour and performance: intermittent locomotion in a climbing fish," *Journal of Zoology*, vol. 277, no. 2, pp. 171–178, 2009.

[7] B. Van Stratum, K. Shoele, and J. Clark, "Reduced order model of lamprey-inspired wall climbing," 2021, ep: 1. [Online]. Available: https://www.dynamicwalking2021.org/episode-1-biomechanics

[8] D. I. Goldman, T. S. Chen, D. M. Dudek, and R. J. Full, "Dynamics of rapid vertical climbing in cockroaches reveals a template," *Journal of Experimental Biology*, vol. 209, no. 15, pp. 2990–3000, 2006.

[9] G. A. Cavagna, N. C. Heglund, and C. R. Taylor, "Mechanical work in terrestrial locomotion: two basic mechanisms for minimizing energy expenditure," *American Journal of Physiology-Regulatory, Integrative and Comparative Physiology*, vol. 233, no. 5, pp. R243–R261, 1977.

[10] R. Blickhan, "The spring-mass model for running and hopping," *Journal of biomechanics*, vol. 22, no. 11-12, pp. 1217–1227, 1989.

[11] S. Hirose and M. Mori, "Biologically inspired snake-like robots," in *2004 IEEE International Conference on Robotics and Biomimetics*. IEEE, 2004, pp. 1–7.

[12] M. Tesch, K. Lipkin, I. Brown, R. Hatton, A. Peck, J. Rembisz, and H. Choset, "Parameterized and scripted gaits for modular snake robots," *Advanced Robotics*, vol. 23, no. 9, pp. 1131–1158, 2009.

[13] G. A. Lynch, J. E. Clark, P.-C. Lin, and D. E. Koditschek, "A bioinspired dynamical vertical climbing robot," *The International Journal of Robotics Research*, vol. 31, no. 8, pp. 974–996, 2012.

[14] C. Hubicki, J. Grimes, M. Jones, D. Renjewski, A. Spröwitz, A. Abate, and J. Hurst, "Atrias: Design and validation of a tether-free 3d-capable spring-mass bipedal robot," *The International Journal of Robotics Research*, vol. 35, no. 12, pp. 1497–1521, 2016.

[15] E. M. Purcell, "Life at low reynolds number," *American journal of physics*, vol. 45, no. 1, pp. 3–11, 1977.

[16] M. J. Lighthill, "Large-amplitude elongated-body theory of fish locomotion," *Proceedings of the Royal Society of London. Series B. Biological Sciences*, vol. 179, no. 1055, pp. 125–138, 1971.

[17] E. Hannigan, B. Song, G. Khandate, M. Haas-Heger, J. Yin, and M. Ciocarlie, "Automatic snake gait generation using model predictive control," in *2020 IEEE International Conference on Robotics and Automation (ICRA)*. IEEE, 2020, pp. 5101–5107.

[18] J. B. Melli, C. W. Rowley, and D. S. Rufat, "Motion planning for an articulated body in a perfect planar fluid," *SIAM Journal on applied dynamical systems*, vol. 5, no. 4, pp. 650–669, 2006.

[19] J. Morison, J. Johnson, and S. Schaaf, "The force exerted by surface waves on piles," *Journal of Petroleum Technology*, vol. 2, no. 05, pp. 149–154, 1950.

[20] D. Tam and A. E. Hosoi, "Optimal stroke patterns for purcell's three-link swimmer," *Physical Review Letters*, vol. 98, no. 6, p. 068105, 2007.

[21] B. Chan, "Bio-inspired fluid locomotion," Ph.D. dissertation, Massachusetts Institute of Technology, Department of Mechanical Engineering, 2009.

[22] S. Alben, "Efficient sliding locomotion with isotropic friction," *Physical Review E*, vol. 99, no. 6, p. 062402, 2019.

[23] R. L. Hatton and H. Choset, "Geometric motion planning: The local connection, stokes' theorem, and the importance of coordinate choice," *The International Journal of Robotics Research*, vol. 30, no. 8, pp. 988–1014, 2011.

[24] Y. Jiao, F. Ling, S. Heydari, E. Kanso, N. Heess, and J. Merel, "Learning to swim in potential flow," *Physical Review Fluids*, vol. 6, no. 5, p. 050505, 2021.

[25] T. Lipták, I. Virgala, P. Frankovskỳ, P. Šarga, A. Gmiterko, and L. Baločková, "A geometric approach to modeling of four-and five-link planar snake-like robot," *International journal of advanced robotic systems*, vol. 13, no. 5, p. 1729881416663714, 2016.

[26] T. Dear, B. Buchanan, R. Abrajan-Guerrero, S. D. Kelly, M. Travers, and H. Choset, "Locomotion of a multi-link non-holonomic snake robot with passive joints," *The International Journal of Robotics Research*, vol. 39, no. 5, pp. 598–616, 2020.

[27] E. Kelasidi, K. Y. Pettersen, J. T. Gravdahl, and P. Liljebäck, "Modeling of underwater snake robots," in *2014 IEEE International Conference on Robotics and Automation (ICRA)*. IEEE, 2014, pp. 4540–4547.

[28] P. Liljebäck, Ø. Stavdahl, K. Y. Pettersen, and J. T. Gravdahl, "Mamba-a waterproof snake robot with tactile sensing," in *2014 IEEE/RSJ International Conference on Intelligent Robots and Systems*. IEEE, 2014, pp. 294–301.

[29] B. J. Van Stratum, K. Shoele, and J. E. Clark, "Lamprey inspired climbing," *IEEE Transactions on Robotics (IN PREPARATION)*, 202X.

[30] J. B. Melli, *A hierarchy of models for the control of fish-like locomotion*. Princeton University, 2008.

[31] U. Saranli, M. Buehler, and D. E. Koditschek, "Design, modeling and preliminary control of a compliant hexapod robot," in *Robotics and Automation, 2000. Proceedings. ICRA'00. IEEE International Conference on*, vol. 3. IEEE, 2000, pp. 2589–2596.